

Dissociation dynamics of the VUV Rydberg states of Xe₂: A velocity map imaging study

*W. Scott Hopkins¹ and Stuart R. Mackenzie,**

Department of Chemistry, University of Oxford, Physical and Theoretical Chemistry
Laboratory, South Parks Road, Oxford, OX1 3QZ, U.K.

Corresponding author:

*stuart.mackenzie@chem.ox.ac.uk

¹Current Address: Department of Chemistry, University of Waterloo, 200 University Avenue
West, Waterloo, Ontario, N2L 3G1, Canada

March 26, 2012

Keywords: xenon dimer, rare gas complexes, Xe₂, Xe₂⁺, photodissociation, velocity map
imaging, van der Waals

Abstract

The photodissociation dynamics of Xe_2 Rydberg states in the 76900 – 80000 cm^{-1} region have been studied using a combination of resonance enhanced multiphoton ionization and velocity map imaging. By monitoring photodissociation product channels as a function of excitation energy, several localized and long range perturbations of the excited states have been identified. In addition, several new band systems have been observed and assigned as the Xe_2 $5d^2[1/2]_0^{\circ} 1_g \leftarrow X 0_g^+$, $5d^2[1/2]_1^{\circ} 2_g \leftarrow X 0_g^+$, $5d^2[3/2]_2^{\circ} 1_g \leftarrow X 0_g^+$, and $5d^2[7/2]_3^{\circ} 0_g^+ \leftarrow X 0_g^+$ transitions.

I. Introduction

The xenon dimer (Xe_2) has been the subject of numerous experimental¹⁻²¹ and theoretical²²⁻³¹ studies owing to its applicability as a gain medium for vacuum ultraviolet (VUV) lasing and as a possible kinetic intermediate in atomic Xe infrared lasers.^{14,32-34} Experimental techniques applied to study Xe_2 have included absorption spectroscopy,^{1,2,11,35} resonance enhanced multi-photon ionization (REMPI),^{3-6,14,18-20} photoelectron spectroscopy,^{7,10,15,16} laser induced fluorescence (LIF),^{9,13,17,21} and, recently, velocity map imaging (VMI).^{8,36,37} For the most part, these experimental studies have focused on the spectroscopic characterization of Rydberg states which correlate with $\text{Xe } 5p^6 (^1\text{S}_0) + \text{Xe}^*$ products, where Xe^* represents excited state xenon in $5p^56s$, $5p^56p$, $5p^55d$, or $5p^57s$ electronic configurations. Numerous curve crossings in this spectral region lead to perturbations in the observed band systems with several states suffering predissociation.^{8,10,13,36,37}

Spectroscopic investigations particularly pertinent to this study have been reported by Dehmer *et al.*,^{3,10} by Gornik *et al.*,^{9,21} and Lipson and coworkers.^{4-7,14,15,19} These investigations involved two-photon excitation of Xe_2 Rydberg states observed *via* photoionization^{3-7,10,14,16,19} or fluorescence.^{9,21} Two-photon transitions in Xe_2 occur between the $X0_g^+$ electronic ground state and the *gerade* excited states. Electric dipole selection rules require that $|\Delta\Omega| \leq 2$, $|\Delta J| \leq 2$, and that $g \leftrightarrow g$ and $+\leftrightarrow +$. Hence, two photon transitions from $X0_g^+$ access only 0_g^+ , 1_g , and 2_g excited states.

Of the eleven potentially accessible molecular states formed from $\text{Xe } 5p^6 (^1\text{S}_0) + \text{Xe}^* 5p^56p$ electronic configurations, six have been characterized spectroscopically with a seventh tentatively assigned as correlating with $\text{Xe } 5p^6 (^1\text{S}_0) + \text{Xe}^* 5p^56p \ ^2[5/2]_2$ products.⁴ Two-photon transitions to these electronic states span the spectral region from 76900 cm^{-1} to 80100

cm^{-1} . Figure 1 summarises the potential energy curves of the 0_g^+ , 1_g , and 2_g Xe_2 excited states observed in the vicinity of the atomic $\text{Xe}^* 5p^5 6p \leftarrow \text{Xe } 5p^6 (^1S_0)$ transitions.

As befits the Rydberg-like nature of these states, their respective potential energy curves (PECs) reflect those of the ion core on which they are based. There are six low-lying electronic states of Xe_2^+ which may contribute to the ion core configuration of the Rydberg states of Xe_2 : $I(^1/_{2u})$, $I(^3/_{2g})$, $I(^3/_{2u})$, $I(^1/_{2g})$, $II(^1/_{2u})$ and $II(^1/_{2g})$. These ion states have respective well depths $D_e^+ = 7934.7 \text{ cm}^{-1} [I(^1/_{2u})]$, $1829.2 \text{ cm}^{-1} [I(^3/_{2g})]$, $453.6 \text{ cm}^{-1} [I(^3/_{2u})]$, $72.9 \text{ cm}^{-1} [I(^1/_{2g})]$, $1422.1 \text{ cm}^{-1} [II(^1/_{2u})]$ and $> 299.4 \text{ cm}^{-1} [II(^1/_{2g})]$.^{38,39} The various excited electronic states of Xe_2 are therefore expected to have a similarly wide range of potential energy well depths and equilibrium bond lengths. Coupled with configuration mixing in Xe_2 excited states,^{23,24,29} it is no surprise that the dissociation dynamics of the xenon dimer are complex.

The $X0_g^+$ ground state of Xe_2 has a shallow van der Waals minimum ($D_e''=195.54 \text{ cm}^{-1}$) at long bond lengths ($r_e''=4.37 \text{ \AA}$).^{12,22} Vertical excitation thus projects the ground state wavefunction onto the region of the outer turning points of many of the excited state PECs (see Figure 1) often leading to significant Franck-Condon overlap with a wide range of excited vibronic states. This leads to a dense spectrum over a wide energy range and provides an excellent means by which to study the photodissociation dynamics of Xe_2 throughout the $76900 - 80000 \text{ cm}^{-1}$ region of the spectrum.

In the present article we report the photodissociation dynamics observed following two-photon excitation of the *gerade* Rydberg states of Xe_2 in the $76900 - 80000 \text{ cm}^{-1}$ region. A combination of resonant multi-photon ionization and velocity map imaging has been used to characterize the prominent dissociation channels leading to a detailed understanding of the several competing processes at play.

II. Experimental

The instrument employed for this study has been described in detail previously but for these studies was operated without the laser ablation metal cluster source.^{40,41} Xe_2 is produced by expanding a 20% mixture of Xe (BOC, 99.999%) in Ar (BOC, >99.9%) from an 8 bar stagnation pressure *via* a pulsed solenoid valve (Parker Hannifin, series 9) into the high vacuum source chamber of a velocity map imaging time-of-flight (VMI-TOF) mass spectrometer.⁴² The resulting molecular beam is skimmed 20 mm downstream of the nozzle orifice with a 1 mm diameter skimmer (Beam Dynamics) before entering the differentially pumped VMI-TOF mass spectrometer region where it is crossed orthogonally by the probe laser mid-way between the VMI repeller and extractor electrodes. Operating pressures in the source and detection chambers are typically 1×10^{-4} mbar and 2×10^{-7} mbar, respectively, with both regions pumped by turbomolecular pumps. These conditions produce excellent signals with little evidence of larger (Xe_n) clusters in either the mass spectrum or the VMI images.

The probe laser system consists of a linearly polarized, frequency-doubled pulsed dye laser (Sirah Cobra Stretch, *ca.* 500 μJ per 8 ns pulse, $\Delta\bar{\nu} \approx 0.30 \text{ cm}^{-1}$) operating with Coumarin 503 laser dye and pumped by the third harmonic of a Nd:YAG laser (Continuum, Surelite II, 10 Hz). Prior to entering the vacuum system, the laser is weakly focused with a $f=200$ mm spherical lens, into the interaction region. The electric field vector of the laser is oriented so as to be parallel to the plane of the MCP / phosphor screen detector.

The instrument can be operated in both in-line linear time-of-flight and velocity map imaging modes. In the former, the mass resolving power is easily capable of distinguishing the different isotopes / isotopologues of Xe / Xe_2 . In VMI mode, photodissociation of Xe_2

leads to spherical shells of Xe fragments in the centre-of-mass frame whose expansion rate is determined by the kinetic energy release in the fragmentation process. Excited state Xe^* photofragments are ionized with an additional photon and the resulting Xe^+ ions are extracted parallel with the molecular beam axis into a 759 mm drift tube and onto a commercial microchannel plate (MCP; 40 mm diameter) detector coupled to a P46 phosphor screen (Photek). Pulsing the rear MCP from +1200 V to +1600 V permits gating of the VMI signal on particular photofragment species of interest, rejecting all other masses. The images are recorded using a 586 x 776 pixel CCD camera, and are analyzed using a purpose-built LabVIEW routine employing the Polar Onion Peeling algorithm of Roberts *et al.*⁴³

III. Results and discussion

Figure 2 gives an overview of the Xe_2 (2+1) REMPI spectrum across the entire region of interest here. The spectroscopy throughout this region has been discussed in considerable detail previously, notably by Dehmer *et al.*³ and Lipson and coworkers,^{4,5,6,7}

A. The $6p\ ^2[1/2]_1\ 1_g \leftarrow X\ 0_g^+$ spectral region

The Xe_2 REMPI spectrum in the region $77000 - 78000\ \text{cm}^{-1}$ is shown in more detail in Figure 3 together with the spectrum recorded simultaneously in the Xe^+ channel. Two weak overlapping band systems are observed, assigned as the $6p\ ^2[1/2]_1\ 1_g \leftarrow X\ 0_g^+$ and the $6p\ ^2[5/2]_2\ 0_g^+ \leftarrow X\ 0_g^+$ electronic transitions by Dimov *et al.*^{5,6} Each vibrational band exhibits structure arising from the 28 naturally occurring isotopologues of Xe_2 .

Every significant feature in the Xe_2 REMPI spectrum is reproduced in the Xe^+ channel indicating the importance of (pre)dissociation processes in the fate of these states. This is most obvious to low wavenumber, where several of the weaker features assigned previously to the $6p\ ^2[1/2]_1\ 1_g\ (\nu'=42-45) \leftarrow X\ 0_g^+\ (\nu''=0)$ progression are more apparent in the Xe^+ fragmentation channel than the Xe_2 REMPI channel.^{5,6} The vibrational spacings for this band system are somewhat irregular, an observation interpreted previously as arising from perturbations of the excited state vibrational levels. This progression merges, around $77200\ \text{cm}^{-1}$, with a stronger band system assigned as $6p\ ^2[5/2]_2\ 0_g^+ \leftarrow X\ 0_g^+\ (\nu'=25-39,0)$, which peaks in intensity at $\nu'=33$.^{5,6} The Xe^+ signal then rises once again as the strong $\text{Xe}\ 5p^5 6p\ ^2[5/2]_2 \leftarrow 5p^6\ [^1S_0]$ atomic resonance at $78119\ \text{cm}^{-1}$ is approached.

Images of the Xe/Xe^+ photofragments were recorded almost continuously across this whole region and several reconstructed images are shown in Figure 3. It is clear from the qualitative differences in these images that the dissociation dynamics differ markedly for different states accessed in this spectral region.

Figure 4 shows the total kinetic energy release (TKER) spectrum obtained from the image recorded following excitation of the $6p\ ^2[1/2]_1\ 1_g \leftarrow X\ 0_g^+ (45,0)$ transition at 77125 cm^{-1} . This TKER spectrum is, in many ways, illustrative of those observed throughout this spectral region. Peaks in the TKER spectrum are observed in three distinct regions: $0 - 1000\text{ cm}^{-1}$, $8000 - 10000\text{ cm}^{-1}$ and $20000 - 26000\text{ cm}^{-1}$ which can be identified with fundamentally different fragmentation processes. The low TKER peaks arise from dissociative ionization at the 3-photon level. By contrast, the highest TKER structure results from direct single-photon dissociation of the Xe_2^+ molecular ion. Both of these processes have been observed in Xe_2 in other spectroscopic regions.^{8,36,37} The peaks in the mid TKER range ($8000 - 10000\text{ cm}^{-1}$) may be assigned conclusively as originating from predissociation of the vibrational levels populated at the two-photon level.

In the $77000 - 77150\text{ cm}^{-1}$ region excitation takes place primarily to the $6p\ ^2[1/2]_1\ 1_g$ ($v'=42-45$) levels. The associated TKER spectra reveal significant predissociation to two distinct product channels. Linear regression of these TKER peaks against the 2-photon wavenumber yields slopes of unity, (indicating dissociation occurs at the two-photon transitions) and intercepts of $67236.4 \pm 7.6\text{ cm}^{-1}$ and $68217.8 \pm 6.2\text{ cm}^{-1}$, which agree well with the $\text{Xe} (^1\text{S}_0) + \text{Xe}^* 5p^5 6s\ ^2[3/2]_2^\circ$ and $\text{Xe}^* 5p^6 (^1\text{S}_0) + \text{Xe} 5p^5 6s\ ^2[3/2]_1^\circ$ dissociation thresholds, respectively. Gaussian fitting of all TKER peaks observed across the entire region of study facilitates the identification of all fragmentation channels and thresholds. A compilation of the TKER spectra for the two-photon channels recorded across the $77,950 - 78,450\text{ cm}^{-1}$ range is shown in Figure 5.

Jonin and Spiegelmann predict four potential energy curves of the correct symmetry and correlating with Xe $5p^6 (^1S_0) + \text{Xe}^* 5p^5 6s \ ^2[3/2]_2^\circ$ and Xe $5p^6 (^1S_0) + \text{Xe}^* 5p^5 6s \ ^2[3/2]_1^\circ$ products to cross the $6p \ ^2[1/2]_1 \ 1_g$ electronic state: $6s \ ^2[3/2]_2^\circ \ 1_g$; $6s \ ^2[3/2]_2^\circ \ 2_g$; $6s \ ^2[3/2]_1^\circ \ 0_g^+$; and $6s \ ^2[3/2]_1^\circ \ 1_g$.²⁴ Each of these has some $6p$ character but the last two exhibit signs of configurational mixing in inflections or “shoulders” occurring in their potential energy curves for $R \leq 3.7$ Å. Further complications arise from an avoided crossing between the $6s \ ^2[3/2]_2^\circ \ 1_g$ and $6s \ ^2[3/2]_1^\circ \ 1_g$ states at ~ 3.3 Å. It is thus tempting to assign the observed $6p \ ^2[1/2]_1 \ 1_g$ predissociation channels to a curve crossing by the $6s \ ^2[3/2]_1^\circ \ 0_g^+$ and/or $6s \ ^2[3/2]_1^\circ \ 1_g$ electronic states. $6s \ ^2[3/2]_2^\circ$ products would then arise from electronic state mixing of $6s \ ^2[3/2]_2^\circ \ 1_g$ and $6s \ ^2[3/2]_1^\circ \ 1_g$. Beyond identifying the final product channels, though, no definitive assignment can be made and all four electronic states remain plausible candidates.

Between 77150 and 77400 cm⁻¹ the $6p \ ^2[1/2]_1 \ 1_g \leftarrow X0_g^+$ and $6p \ ^2[5/2]_2 \ 0_g^+ \leftarrow X0_g^+$ band systems overlap and the complex nature of Xe₂ excited state dissociation is manifest in several observations. The $6p \ ^2[1/2]_1 \ 1_g \leftarrow X0_g^+$ band system apparently terminates rather abruptly at ~ 77125 cm⁻¹ with the (45,0) transition, well short of the Xe $5p^6 (^1S_0) + \text{Xe}^* 5p^5 6p \ ^2[1/2]_1$ asymptote at ~ 77455 cm⁻¹. Above 77125 cm⁻¹, all observed transitions can be assigned to the $6p \ ^2[5/2]_2 \ 0_g^+ \leftarrow X0_g^+ (v',0)$ system. No dramatic changes are observed in the Xe images in this region (see Figure 3) suggesting either that the same predissociation mechanism as above applies and/or that the Xe₂ states in this region are of mixed $6p \ ^2[1/2]_1 \ 1_g / 6p \ ^2[5/2]_2 \ 0_g^+$ character.

The first significant change in the predissociation dynamics occurs upon opening of the Xe $5p^6 (^1S_0) + \text{Xe}^* 5p^5 6s \ ^2[1/2]_1^\circ$ channel at 77371 cm⁻¹ degenerate with the $6p \ ^2[5/2]_2 \ 0_g^+ \leftarrow X0_g^+ (28,0)$ transition. Above this energy no Xe $^* 5p^5 6s \ ^2[3/2]_1^\circ$ products are observed and the branching ratio into the Xe $^* 5p^5 6s \ ^2[3/2]_2^\circ$ product channel is much diminished. Between

the Xe $5p^6 [^1S_0] + \text{Xe}^* 5p^5 6s \ ^2[1/2]_1^\circ$ threshold and the Xe $5p^6 [^1S_0] + \text{Xe} 5p^5 6p \ ^2[1/2]_1$ threshold at 77455 cm⁻¹, the major dissociation products at the two-photon level are low TKER products corresponding to the Xe $5p^6 [^1S_0] + \text{Xe}^* 5p^5 6s \ ^2[1/2]_1^\circ$ channel. This is unsurprising as Xe $5p^6 [^1S_0] + \text{Xe}^* 5p^5 6s \ ^2[1/2]_1^\circ$ atomic states correlate with 1_g and 0_g^+ molecular states, the dissociative continua of which can both couple with the $6p \ ^2[5/2]_2 \ 0_g^+$ and $6p \ ^2[1/2]_1 \ 1_g$ states populated. More surprising is that immediately above the Xe $5p^6 [^1S_0] + \text{Xe}^* 5p^5 6p \ ^2[1/2]_1$ threshold, *all* dissociation into the Xe $5p^6 [^1S_0] + \text{Xe}^* 5p^5 6s \ ^2[3/2]_2^\circ$ product channel disappears in favour of low TKER photofragments – predominantly the Xe $5p^6 [^1S_0] + \text{Xe}^* 5p^5 6p \ ^2[1/2]_1$ channel, with a minor contribution from Xe $5p^6 [^1S_0] + \text{Xe}^* 5p^5 6s \ ^2[1/2]_1^\circ$ products.

Additional information on the dissociation processes in the region of these thresholds may be gleaned from the anisotropy of the VMI images. Figure 6 shows the low TKER region of the reconstructed image acquired following excitation of the $^{129}\text{Xe}^{132}\text{Xe} \ 6p \ ^2[5/2]_2 \ 0_g^+ (v'=29)$ level. This level lies just below the Xe $5p^6 [^1S_0] + \text{Xe}^* 5p^5 6p \ ^2[1/2]_1$ threshold and the low TKER peak ($\approx 80 \text{ cm}^{-1}$) corresponds to dissociation into the Xe $5p^6 [^1S_0] + \text{Xe}^* 5p^5 6s \ ^2[1/2]_1^\circ$ channel. The clear $\sin^2\theta\cos^2\theta$ distribution in the image is indicative of prompt dissociation following a two-photon $1_g \leftarrow 0_g^+$ transition.⁴⁴ This suggests that the $6p \ ^2[5/2]_2 \ 0_g^+ v'=29$ state has significant 1_g character which could arise either by mixing with the bound $6p \ ^2[1/2]_1 \ 1_g$ state or *via* coupling with the $6s \ ^2[1/2]_1^\circ \ 1_g$ continuum. It is also interesting to note the distinct difference between this $\sin^2\theta\cos^2\theta$ angular distribution and the near isotropic distributions observed for the Xe $5p^6 ({}^1S_0) + \text{Xe}^* 5p^5 6s \ ^2[3/2]_2^\circ$ and Xe $5p^6 ({}^1S_0) + \text{Xe}^* 5p^5 6s \ ^2[3/2]_1^\circ$ product channels (see Figure 3). This suggests that below the Xe $5p^6 [^1S_0] + \text{Xe}^* 5p^5 6s \ ^2[1/2]_1^\circ$ threshold the $6p \ ^2[5/2]_2 \ 0_g^+$ and $6p \ ^2[1/2]_1 \ 1_g$ states are relatively long-lived compared with the rotational period (*i.e.*, $\tau > \text{ps}$) whereas between the Xe $5p^6 [^1S_0] + \text{Xe}^* 5p^5 6s \ ^2[1/2]_1^\circ$ and Xe $5p^6 [^1S_0] + \text{Xe}^* 5p^5 6p \ ^2[1/2]_1$ thresholds the bound states of Xe₂ are strongly coupled with the

newly opened dissociation channel. The supplementary material accompanying this article contains details of the anisotropy parameters extracted from all velocity map images.⁴⁵

B. The $6p\ ^2[5/2]_2\ 0_g^+ \leftarrow X\ 0_g^+$ spectral region

From 77450 – 78000 cm⁻¹ the Xe₂ REMPI spectrum is dominated by transitions to the $6p\ ^2[5/2]_2\ 0_g^+ \leftarrow X\ 0_g^+$ band system.^{3-7,10} Observed peak positions are in good agreement with those reported by Dimov *et al.*⁵ As discussed above, predissociation of the $6p\ ^2[5/2]_2\ 0_g^+$ ($v'=25-27$) levels yields products similar to those observed following excitation of the $6p\ ^2[1/2]_1\ 1_g$ $v'=42-45$ states. However, as soon as the Xe* $5p^56s\ ^2[1/2]_1^\circ$ dissociation threshold opens (around $6p\ ^2[5/2]_2\ 0_g^+$ $v'=28-29$) this becomes the dominant product channel.

A similarly abrupt change in the photofragment branching ratio is also observed at the Xe $5p^6\ [^1S_0] + \text{Xe}\ 5p^56p\ ^2[1/2]_1$ threshold ($\sim 77455\text{ cm}^{-1}$). Just below this threshold, photofragment products are partitioned approximately 9:1 in favour of (low-TKER) Xe* $5p^56s\ ^2[1/2]_1^\circ$ products over (mid-TKER) Xe* $5p^56s\ ^2[3/2]_2^\circ$ products. Above the threshold, however, Xe* $5p^56p\ ^2[1/2]_1$ products are predominantly observed with no production of Xe* $5p^56s\ ^2[3/2]_2^\circ$ products and only a minor contribution from the Xe* $5p^56s\ ^2[1/2]_1^\circ$ product channel (see Figure 5). The only molecular state predicted to occur in this spectral region that correlates with Xe $5p^6\ [^1S_0] + \text{Xe}^*\ 5p^56p\ ^2[1/2]_1$ atomic states, and which can interact with the (pure) $6p\ ^2[5/2]_2\ 0_g^+$ state, is the $6p\ ^2[1/2]_1\ 1_g$ state.²⁴ We therefore suggest that the bound levels of the $6p\ ^2[5/2]_2\ 0_g^+$ state are directly coupled to the $6p\ ^2[1/2]_1\ 1_g$ dissociative continuum. This coupling apparently persists for *ca.* 100 cm⁻¹ above the Xe $5p^6\ [^1S_0] + \text{Xe}^*\ 5p^56p\ ^2[1/2]_1$ threshold. In this region, Xe images of the low TKER, Xe $5p^6\ [^1S_0] + \text{Xe}^*\ 5p^56p\ ^2[1/2]_1$ product channel, display a $\sin^2\theta\cos^2\theta$ angular distribution similar to that in Figure 6 again consistent with

prompt dissociation *via* the $6p\ ^2[1/2]_1\ 1_g$ dissociative continuum. At higher excitation energies the Xe $5p^6\ [^1S_0] + \text{Xe}^*\ 5p^5 6s\ ^2[1/2]_1^\circ$ product channel becomes dominant once more.

The Xe $5p^6\ (^1S_0) + \text{Xe}^*\ 5p^5 6s\ ^2[3/2]_2^\circ$ product channel is again observed briefly between 77720 and 77890 cm⁻¹ this time in a branching ratio of approximately 1:4 with the Xe $5p^6\ [^1S_0] + \text{Xe}^*\ 5p^5 6s\ ^2[1/2]_1^\circ$ channel. There are a number of potential perturber states which may be implicated but the relatively high $6p$ character of the $6s\ ^2[3/2]_1^\circ\ 1_g$ state makes it a strong candidate.²⁴

C. The $6p\ ^2[5/2]_2\ 2_g \leftarrow X\ 0_g^+$ spectral region

Figure 7A shows the Xe₂ REMPI spectrum covering the spectral region in the vicinity of the atomic Xe $5p^5 6p\ ^2[5/2]_2 \leftarrow 5p^6\ (^1S_0)$ transition at 78119.798 cm⁻¹. The two most intense transitions in this region have been assigned previously to the $6p\ ^2[5/2]_2\ 2_g \leftarrow X0_g^+$ (0,0) and (1,0) bands in studies which have commented on the dissociative dynamics of the $6p\ ^2[5/2]_2\ 2_g\ v' = 0$ state.^{3,7,8,10} Some of the weaker features have been noted previously,^{3,4} but many are observed here for the first time. These peaks are definitely Xe₂ REMPI transitions, VMI studies ruling the possibility of fragmentation of higher order clusters. Likewise Xe⁺ images show only the sharp TKER peaks expected for diatomic dissociation (see Figure 7B).

Two possible band systems can be identified based on band profiles and peak separations in the 78100 – 78400 cm⁻¹ region (see Figure 7a). The peak separations in these progressions are *ca.* 35–40 cm⁻¹, *i.e.*, ~170% larger than that expected for the $6p\ ^2[5/2]_2\ 1_g$ state ($\Delta G_{1/2} \approx 21\text{ cm}^{-1}$). It seems more likely that these bands are associated with the $5d\ ^2[1/2]_0^\circ\ 1_g \leftarrow X0_g^+$ and $5d\ ^2[1/2]_1^\circ\ 2_g \leftarrow X0_g^+$ band systems. This assignment is further supported by the observed TKER spectra (see Figure 7b). For both band systems no dissociation into the Xe $5p^6\ [^1S_0] + \text{Xe}^*\ 6s$

$2[3/2]_2^\circ$ channel is observed and the high TKER region (associated with photodissociation of the molecular ion) is much more densely structured.

The complex nature of excited state mixing and predissociation throughout this region is exemplified by the low TKER product channels. The observed angular distribution for the Xe $5p^6 [^1S_0] + \text{Xe}^* 5p^5 6p^2 [1/2]_1$ product channel (TKER $\approx 600 \text{ cm}^{-1}$), following dissociation *via* the $6p^2 [5/2]_2 2_g v' = 0$ state apparently shows a clear $\cos^2 2\theta$ dependence (see inset Figure 7b). This is not a limiting case for a two-photon recoil anisotropy, but Dixon has shown that if the transition tensors for $\Sigma \rightarrow \Sigma \rightarrow \Sigma$ and $\Sigma \rightarrow \Pi \rightarrow \Sigma$ two-photon pathways contribute with equal but opposite amplitudes, the sum is proportional to $\cos 2\theta$, and thus $P(\theta) = \cos^2 2\theta$.⁴⁴ Although the body-fixed axial angular momentum was treated using a Hund's case (b) basis in Dixon's study, the same theory will apply to the likely Hund's case (c) coupling in Xe₂. This might suggest a prompt dissociation *via* a 0_g^+ excited state,⁴⁴ rather than the 2_g assignment of Dimov *et al.*⁶ but predissociation is a minor channel compared with ionization.

Xe⁺ images recorded *via* the $6p^2 [5/2]_2 2_g v' = 1$ state reveal predissociation into the same two channels as *via* the $v'=0$ level. In this instance, however, dissociation into both product channels exhibit strongly anisotropic photofragment distributions peaked perpendicular to the laser polarization vector, indicative of prompt dissociation *via* a $\Sigma \rightarrow \Pi \rightarrow \Sigma$ or $\Sigma \rightarrow \Pi \rightarrow \Delta$ transition (0_g^+ or 2_g states).⁴⁴

The (L,0) peak at $\sim 78055 \text{ cm}^{-1}$ occurs at the expected wavenumber for the (2,0) transition but has been assigned to another electronic transition.⁴ The velocity map images bear this out with the $5p^5 6s^2 [1/2]_1^\circ$ channel now exhibiting an essentially isotropic angular distribution. Finally, predissociation *via* the band systems above 78100 cm^{-1} generates only Xe $5p^6 [^1S_0] + \text{Xe}^* 5p^5 6s^2 [1/2]_1^\circ$ products with approximately $\sin^2 \theta \cos^2 \theta$ angular distributions, except for the (N,0) transition which has significant $\cos^2 \theta$ component (*i.e.*, $\beta_2 > 0$) as well.

D. The $6p\ ^2[3/2]_2\ 2_g / ^2[3/2]_2\ 1_g \leftarrow X0_g^+$ spectra region

The Xe₂ spectrum in the region of the atomic Xe $5p^5 6p\ ^2[3/2]_2 \leftarrow 5p^6\ (^1S_0)$ transition is shown in Figure 8. The intense $6p\ ^2[3/2]_2\ 2_g \leftarrow X0_g^+$ and $6p\ ^2[3/2]_2\ 1_g \leftarrow X0_g^+$ systems are observed in both the Xe₂⁺ REMPI mass channel and dissociative Xe⁺ mass channel.^{3,5-7} The $6p\ ^2[3/2]_2\ 1_g \leftarrow X0_g^+$ transition is much the more intense in the Xe⁺ channel indicating the $6p\ ^2[3/2]_2\ 1_g$ state to be more strongly predissociative than the $6p\ ^2[3/2]_2\ 2_g$ state. The dynamics of these states have been studied previously,^{7,8,10} most recently in a VMI study by Schubert *et al.* wherein the authors identified two dissociation channels active in both band systems: Xe (¹S₀) + Xe* $6p\ ^2[5/2]_2$ and Xe (¹S₀) + Xe* $6p\ ^2[5/2]_3$.⁸

A few members of a weaker third band system are also observed in the Xe⁺ mass channel in the region 78500 – 78800 cm⁻¹. Line spacings (*ca.* 48 cm⁻¹) suggest the excited Rydberg state has a I(3/2g) ion core,^{7,39} while band profiles (*viz.* widths due to the vibrational isotope effect) indicate that the levels accessed are of relatively low vibrational excitation (*v'* ≈ 15). NO conclusive assignment is possible but the 1_g or 2_g states associated with the Xe* $5d\ ^2[3/2]_2^\circ + \text{Xe} (^1S_0)$ threshold are the most likely candidates for the excited state.

Due to the spectral density in this region, Xe images could be acquired pseudo-continuously across the 78500 – 79100 cm⁻¹ region. All images observed contained low-TKER rings (*ca.* 2500 cm⁻¹), which can be assigned to predissociation and dissociative ionization of neutral Xe₂, and very high TKER rings (> 21000 cm⁻¹) assigned to Xe₂⁺ photodissociation, consistent with the observations of Shubert *et al.*^{8,37} Regression of the low TKER peaks with excitation energy confirms their assignment as predissociation at the two-photon level yielding Xe* $6p\ ^2[5/2]_2$ and Xe* $6p\ ^2[5/2]_3$ products (see Figure 9A, B).

Spectral congestion precludes exclusive excitation of only one of either the $6p^2[3/2]_2 1_g \leftarrow X0_g^+$ or $6p^2[3/2]_2 2_g \leftarrow X0_g^+$ transitions but where adjacent features are most separated, the low TKER region of the observed Xe images exhibit somewhat different dissociation dynamics: Whilst excitation of the $6p^2[3/2]_2 2_g$ vibronic levels produces $\text{Xe}^* 6p^2[5/2]_3$ and $\text{Xe}^* 6p^2[5/2]_2$ products in a 3:1 ratio, the $6p^2[3/2]_2 1_g$ vibronic levels display a marked propensity for producing $\text{Xe}^* 6p^2[5/2]_2$. Figure 9 C,D compares the images and TKER spectra acquired following excitation of the $^{132}\text{Xe}^{132}\text{Xe } 6p^2[3/2]_2 2_g (\nu'=4)$ and $6p^2[3/2]_2 1_g (\nu'=29)$ states, which are separated by approximately 10 cm^{-1} and are relatively free of blending. The slightly parallel angular product distribution observed from the $6p^2[3/2]_2 1_g (\nu'=29)$ state is consistent a $\Sigma \rightarrow \Sigma \rightarrow \Pi$ or $\Sigma \rightarrow \Pi \rightarrow \Pi$ excitation scheme.⁴⁴ However, the similarly parallel distribution from the $6p^2[3/2]_2 2_g (\nu'=4)$ state, is inconsistent with the negative β_2 parameter expected following $\Sigma \rightarrow \Pi \rightarrow \Delta$ excitation. Rather, this state is more likely of 1_g symmetry or 0_g^+ symmetry accessed *via* a $\Sigma \rightarrow \Sigma \rightarrow \Sigma$ excitation scheme.⁴⁴ Similar observations within this band system have been previously attributed to electronic state mixing with the $6p^2[3/2]_2 1_g$ state.⁸

At excitations below $\sim 78850 \text{ cm}^{-1}$ three product channels $\text{Xe } ({}^1S_0) + \text{Xe}^* = 6p^2[5/2]_2, 6p^2[5/2]_3$ and $6s^2[1/2]_2^o$, respectively are observed in the low TKER range. Where these product channels are observed, $\text{Xe}_2 6p^2[3/2]_2 1_g \leftarrow X0_g^+$ transitions can be identified in the Xe^+ mass channel along with the newly observed band system (see Figure 8). Again, selective excitation of only one of these band systems proved difficult but velocity map images and TKER spectra following excitation of $6p^2[3/2]_2 1_g (\nu'=22)$ and the $(\nu'=m+2)$ state of the new band system are shown in Figure 10. The $\sin^2\cos^2\theta$ angular distributions observed in each are clear and consistent with prompt dissociation following a two photon $1_g \leftarrow 0_g^+$ excitation.⁴⁴ Unlike $6p$

$^2[3/2]_2$ 1_g levels, excitation of $5d$ $^2[3/2]_2$ 1_g bands does not produce high TKER Xe⁺ from Xe₂⁺ photolysis as REMPI to form Xe₂⁺ is only a very minor process.

Figure 11 provides a summary of the low TKER product channels observed throughout the 78500 – 79200 cm⁻¹ region. Interestingly, despite it being identified as a predissociative product channel in the photoelectron spectrum, nowhere we did not observe dissociation to the Xe* $6p$ $^2[1/2]_1$ + Xe (1S_0) threshold.¹⁰ Two product channels assigned to photodissociation of ArXe were observed in this region and will be reported elsewhere.

E. The Xe $5p^5 5d$ $^2[1/2]_1$ $^\circ \leftarrow 5p^6$ (1S_0) Spectral Region

Figure 12A shows the Xe₂ REMPI spectrum in the region of the Xe $5p^5 5d$ $^2[1/2]_1$ $^\circ \leftarrow 5p^6$ (1S_0) atomic transition. The intense $0_g^+ \leftarrow X0_g^+$ Xe₂ band system dominating the region has been studied previously^{5,7} and based on vibrational spacing and the dominant I(3/2u) ion core configuration,⁷ it seems likely to be the 0_g^+ associated with the Xe* $5p^5 6p$ $^2[1/2]_0$ + Xe $5p^6$ (1S_0) threshold. However, the complex photoelectron spectra and photoelectron images recorded from these levels reflect the strongly mixed character of the Rydberg core.^{10,37} We observe an additional band system to the red of the documented transitions. Vibrational spacings (*ca.* 58 cm⁻¹) and band profiles suggest these are transitions to relatively low v' members of either the $5d$ $^2[7/2]_3$ $^\circ 0_g^+$, $5d$ $^2[3/2]_2$ $^\circ 1_g$, or $5d$ $^2[3/2]_2$ $^\circ 2_g$ states.

The low kinetic energy dissociation products following excitation *via* the $6p$ $^2[1/2]_0$ 0_g^+ state at *ca.* 79610 cm⁻¹ have been discussed previously.⁸ Briefly, two product channels associated with predissociation forming Xe* $6p$ $^2[3/2]_2$ and Xe* $6p$ $^2[5/2]_3$ are observed, along with broad features assigned to dissociative ionization. The same fragment channels are observed *via* the new ($v' = n+1-3$) $\leftarrow X0_g^+$ vibronic bands the relative branching ratios varying significantly across the band system. Figures 12B-D show the low TKER regions of the

images acquired from the ($v' = n+1-3$) states. Excitation of the ($v' = n+1$) state produces Xe_2^* marginally below the $\text{Xe}^* 6p^2[3/2]_2 + \text{Xe} (^1S_0)$ threshold at 79398.5 cm^{-1} (marked on Figure 12A with a dashed line), and produces $\text{Xe}^* 6p^2[5/2]_3 + \text{Xe} (^1S_0)$ products. By contrast, excitation of the ($v' = n+2,3$) states, which lie just above the threshold, results in nearly exclusive coupling to the newly opened product channel.

Excitation of Xe_2 to the ($v' = n+1-3$) levels generates product angular distributions peaked perpendicular to the laser polarization vector (see inset figures 12B-D) consistent with $\Sigma \rightarrow \Pi \rightarrow \Delta$ or $\Sigma \rightarrow \Pi \rightarrow \Sigma$ excitation,⁴⁴ followed by prompt dissociation. Given the observation of the $5d^2[3/2]_2^{\circ} 1_g \leftarrow X0_g^+$ transition at $\sim 78500 \text{ cm}^{-1}$ (see section III.D), it might be expected that transitions to the $5d^2[3/2]_2^{\circ} 2_g$ state should occur at similar excitation energies. We thus favour a $5d^2[7/2]_3^{\circ} 0_g^+$ excited state assignment for the transitions observed in the $79300 - 79600 \text{ cm}^{-1}$ region. However, given mixing observed for the more intense 0_g^+ excited state in this region, a definitive assignment of the weak band system cannot be made.⁸

IV Summary and Conclusions

The photodissociation dynamics of Xe_2 across the $76900 - 80000 \text{ cm}^{-1}$ spectral region are varied and complex. Photofragment images, however, recorded following excitation of numerous vibronic levels provide a detailed picture of predissociative mechanisms and curve crossings for the excited state potentials. Highly localized perturbations caused by potential energy curve crossings are observed as abrupt changes in product state distributions over very narrow spectral regions (*e.g.*, $6p^2[5/2]_2 0_g^+ v' = 35, 36$). Such observations provide an excellent measure by which to test theoretical predictions. The identical predissociation products and angular distributions observed for the $6p^2[1/2]_1 1_g v' \approx 42-50$ and $6p^2[5/2]_2 0_g^+ v' \approx 20-29$ states reflect the importance of electronic state mixing in Xe_2 $6p$ Rydberg states. However, the

observed *differences* in the photodissociation products for the $6p\ ^2[3/2]_2\ 2_g$, $^2[3/2]_2\ 1_g$, and $5d\ ^2[3/2]_2\ ^\circ\ 1_g$ states (despite their close proximity) suggests that employing VMI to gate on signature product channels may provide an effective means to disentangle highly congested spectra.

This combined spectroscopic and chemical dynamic approach has lead to the assignment of four newly observed Xe_2 electronic transitions, for which the associated excited states are $5d\ ^2[1/2]_0\ ^\circ\ 1_g$ (*ca.* 78120 cm^{-1}), $5d\ ^2[1/2]_1\ ^\circ\ 2_g$ (*ca.* 78120 cm^{-1}), $5d\ ^2[3/2]_2\ ^\circ\ 1_g$ (*ca.* 78600 cm^{-1}) and $5d\ ^2[7/2]_3\ ^\circ\ 0_g^+$ (*ca.* 79300 cm^{-1}). These assignments are also consistent with the relative spectral intensities for the Xe_2 transitions observed throughout the 76900 – 80000 cm^{-1} region, where molecular transitions associated with (two-photon) allowed $6p \leftarrow 5p$ atomic Xe transitions are much more intense than those associated with forbidden $5d \leftarrow 5p$ atomic Xe transitions.

Acknowledgements

The authors would like to thank Mr. Alex Woodham for help during the data acquisition. Funding for this research was provided by the Engineering and Physical Sciences Research Council (EPSRC, grant EP/C012070). WSH acknowledges funding from the Ramsay Memorial Fellowships Trust in the form of a Ramsay Memorial Fellowship.

Figure Captions

- Figure 1 Potential energy curves for the xenon dimer, Xe_2 , in the region of the atomic $6p$ and $5d$ excited states. Potential energy curves are based on Morse potential parameters reported in the literature, with equilibrium bond lengths slightly adjusted to yield Franck-Condon envelopes consistent with observed intensity profiles.^{4,5,14}
- Figure 2 Overview of the Xe_2 (2+1) REMPI spectrum in the region of the $5p^5 6p$ Rydberg states. Assignments are taken from refs 2-6. Dashed vertical lines indicated excited states in atomic Xe.
- Figure 3 The Xe_2 (2+1) REMPI spectrum in the region of the $6p^2 [^1/2]_1 1_g \leftarrow X0_g^+$ and $6p^2 [^5/2]_2 0_g^+ \leftarrow X0_g^+$ transitions as observed in the Xe_2^+ (upper) and Xe^+ (lower) mass channels. (Inset; bottom) The reconstructed Xe^+ ion images acquired following photolysis *via* the various Xe_2 transitions (indicated with arrows).
- Figure 4 The TKER spectrum observed following excitation of the $6p^2 [^1/2]_1 1_g \leftarrow X0_g^+$ (45,0) transition. Three distinct regions can be identified: dissociative ionization (low TKER), predissociation of the excited neutral level (mid TKER) and photodissociation of Xe_2^+ (high TKER).
- Figure 5 A. The observed TKER peak positions for the predissociation channels of Xe_2 in the $76900 - 79500 \text{ cm}^{-1}$ region. The observed product channels are: $\text{Xe} (^1\text{S}_0) + \text{Xe}^* 6s^2 [3/2]_2^o$ (green circles), $\text{Xe} (^1\text{S}_0) + \text{Xe}^* 6s^2 [3/2]_1^o$ (red squares), $\text{Xe} (^1\text{S}_0) + \text{Xe}^* 6s^2 [1/2]_1^o$ (blue triangles) and $\text{Xe} (^1\text{S}_0) + \text{Xe}^* 6p^2 [1/2]_1$ (orange triangles). Dissociation thresholds are indicated with horizontal dashed lines. B. Compilation

of the TKER spectra for the predissociation channels recorded across the whole range investigated in this study.

Figure 6 A. The low TKER region of the reconstructed image acquired following excitation of the Xe_2 $6p\ ^2[5/2]_2\ 0_g^+ \leftarrow X0_g^+$ (29,0) transition. The polarization vector (\underline{E}) of the photolysis laser is vertical with respect to the image. B. 3D contour plot of the image shown in A. C. The angular intensity distribution of the image shown in A. and B. The curve shows a fitted Legendre polynomial function including 2nd and 4th order anisotropy parameters.

Figure 7 A. The Xe_2 (2+1) REMPI spectrum in the region of the atomic Xe $6p\ ^2[5/2]_2 \leftarrow ^1S_0$ transition. Weak features marked with an asterisk (*) can be assigned to $v'' = 1$ hot bands associated with the more intense $v'' = 0$ transitions to slightly higher wavenumber. B. Selected TKER spectra extracted from Xe^+ images recorded from the Xe_2 REMPI transitions indicated on the spectra. Corresponding images are shown to the right of the spectra, while a magnified view of the low TKER predissociative product channel for each spectrum is shown inset. The photolysis laser polarization vector (\underline{E}) was vertical with respect to the plotted image.

Figure 8 Xe_2 spectrum in the region of the $\text{Xe}^* 6p\ ^2[3/2]_2$ state as observed in the Xe_2^+ (top panel) and Xe^+ (bottom panel) mass channels. The intense $6p\ ^2[3/2]_2\ 2_g \leftarrow X0_g^+$ and $6p\ ^2[3/2]_2\ 1_g \leftarrow X0_g^+$ Xe_2 band systems are indicated with an assignment comb. An additional band system, assigned as $(v'=m+0-5,0)$ transitions (bottom panel), is also indicated. Asterisks mark the positions at which the images in Figure 9C,D were taken.

Figure 9 TKER peak positions as a function of excitation wavenumber for relatively unblended features of the A. $6p\ ^2[3/2]_2\ 1_g \leftarrow X0_g^+$ and B. $6p\ ^2[3/2]_2\ 2_g \leftarrow X0_g^+$

band systems. Xe velocity map images and extracted low TKER spectra observed following excitation of the C. $6p\ ^2[3/2]_2\ 2_g\ (\nu'=4)$ and D. $6p\ ^2[3/2]_2\ 1_g\ (\nu'=29)$ vibronic levels.

Figure 10 Xe velocity map images and extracted low TKER spectra observed following excitation of the A. $6p\ ^2[3/2]_2\ 1_g\ (\nu'=22)$ and B. $(\nu'=m+2)$ vibronic levels.

Figure 11 (Top panel) The Xe_2 spectrum in the $78500 - 79100\ \text{cm}^{-1}$ as observed in the Xe^+ mass channel. (Bottom panel) The low Xe TKER peaks observed in the $78500 - 79100\ \text{cm}^{-1}$ region. Solid lines show the predicted Xe TKER wavenumber dependence for two-photon dissociation of Xe_2 , while dashed lines show the predicted dependence for two-photon dissociation of ArXe .

Figure 12 A. The $\text{Xe}_2\ (2+1)$ REMPI spectrum in the $79250 - 79900\ \text{cm}^{-1}$ region as observed in the Xe_2^+ mass channel. The $0_g^+ \leftarrow X0_g^+$ assignment is from references 5,6. (Inset) a $\times 20$ multiplication of the $79250 - 79550\ \text{cm}^{-1}$ region where an additional band system assigned as $(\nu'=n+0-4,0)$ transitions is observed. B-D. Xe velocity map images and extracted low TKER spectra observed following excitation of the B. $(\nu'=n+3)$, C. $(\nu'=n+2)$ and D. $(\nu'=n+1)$ vibronic levels.

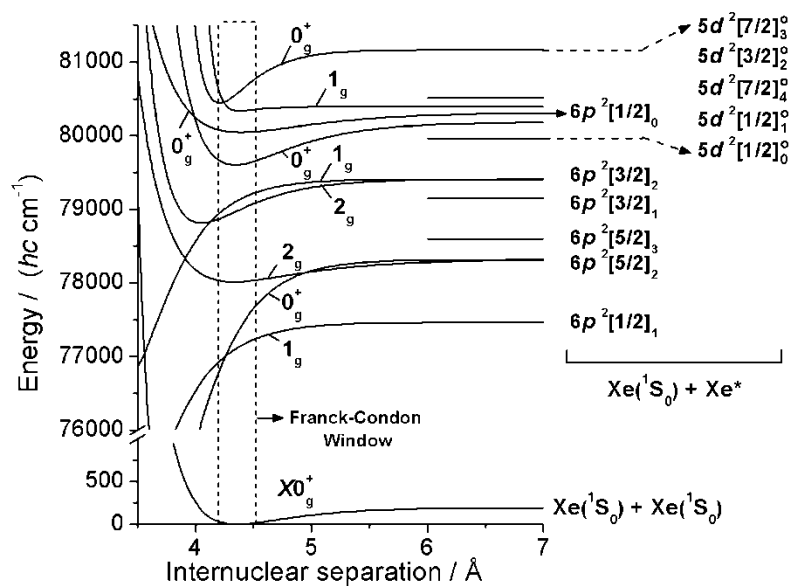


Figure 1

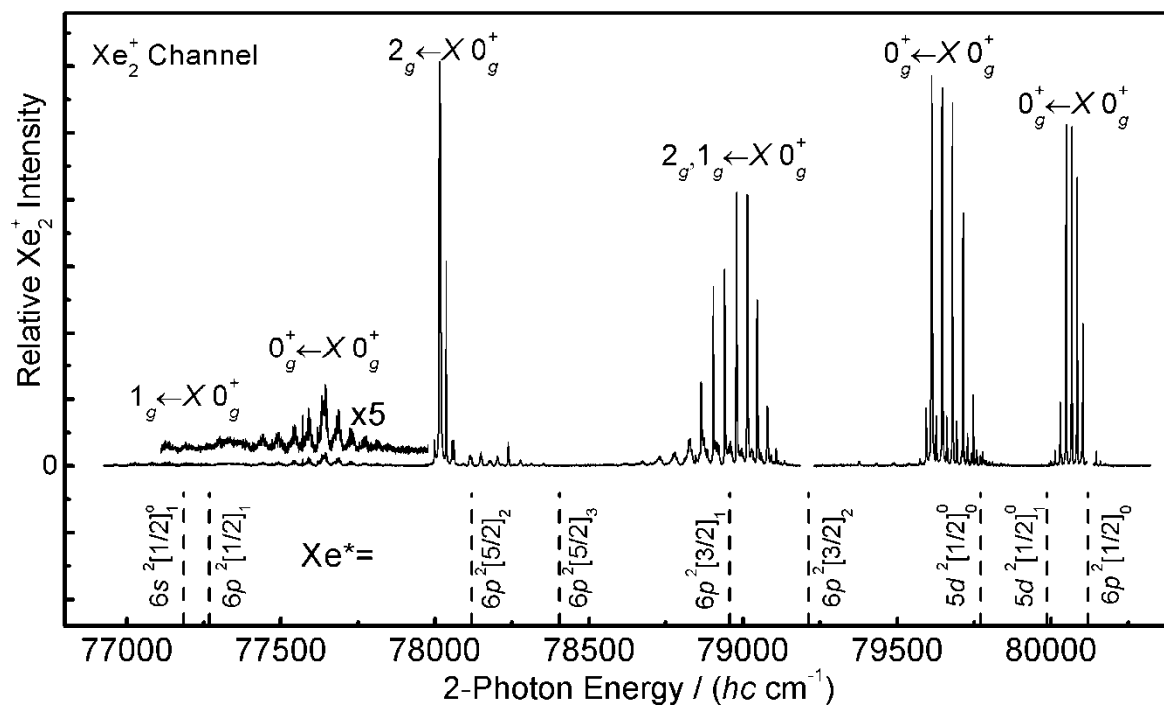


Figure 2

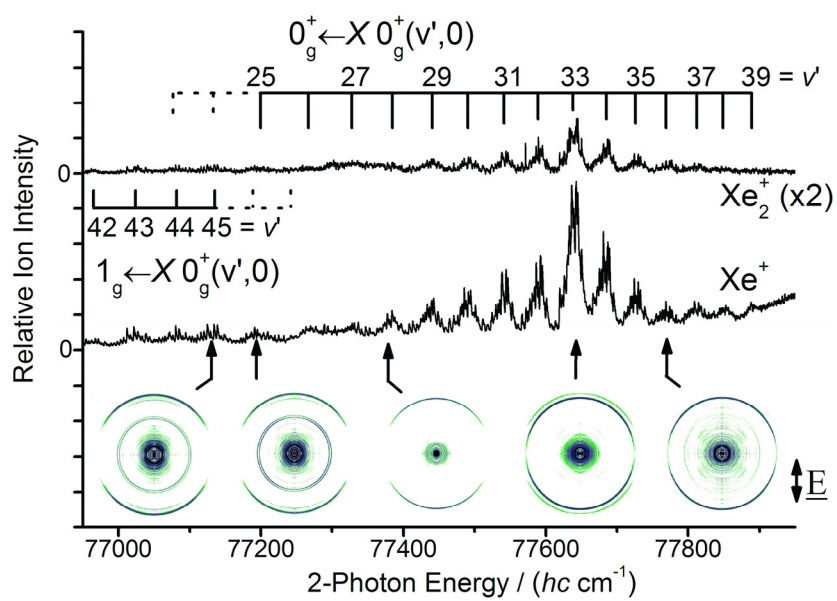


Figure 3

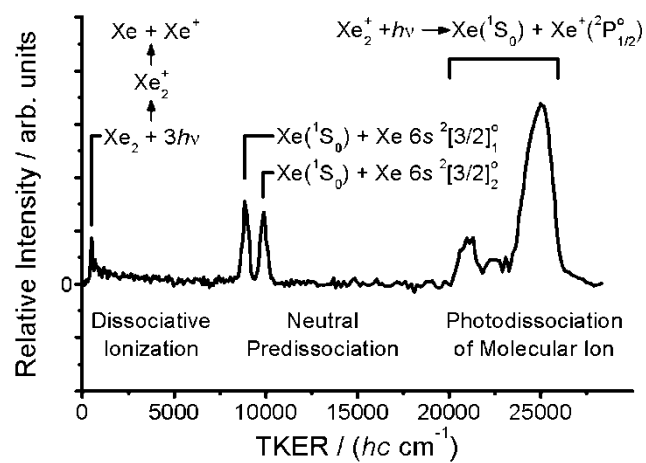


Figure 4

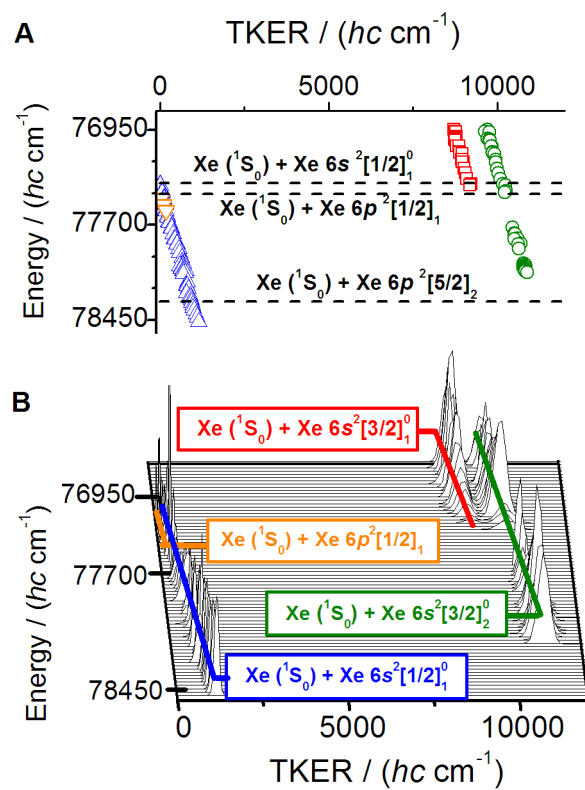


Figure 5

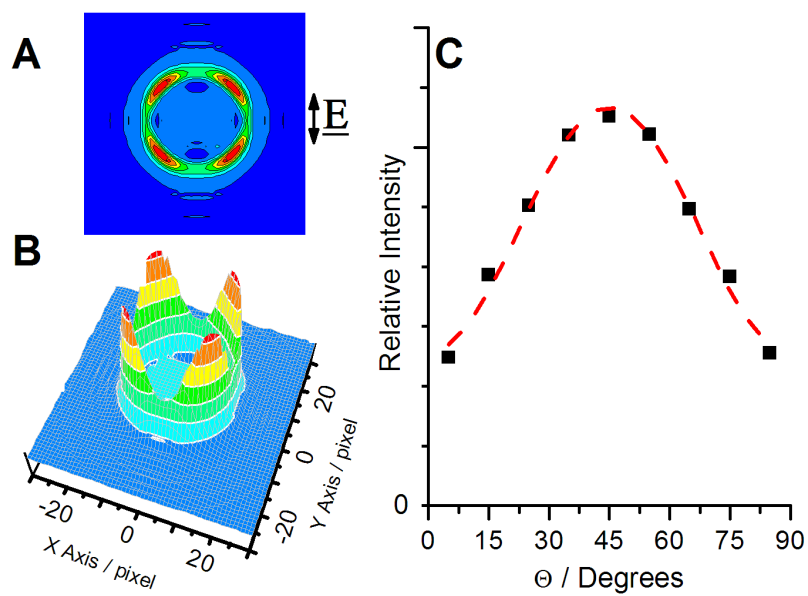


Figure 6

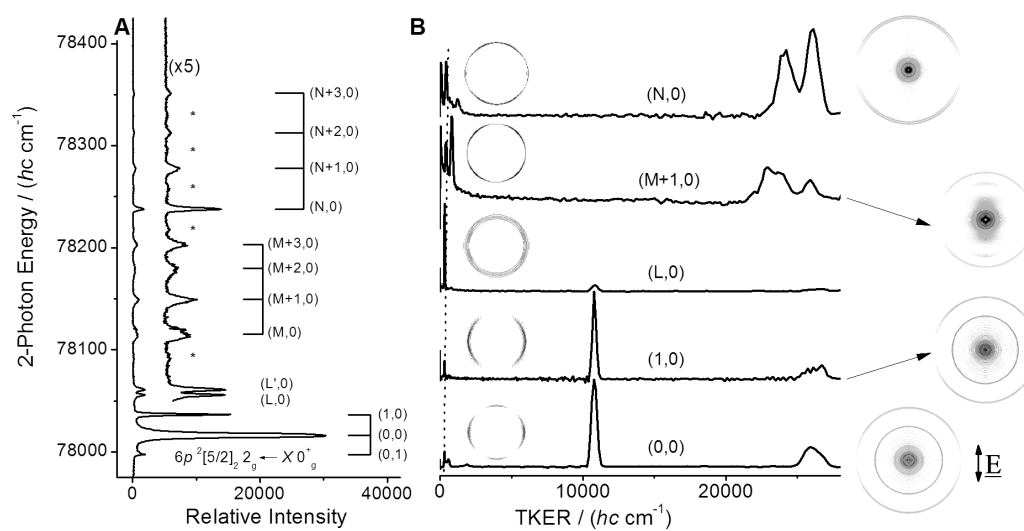


Figure 7

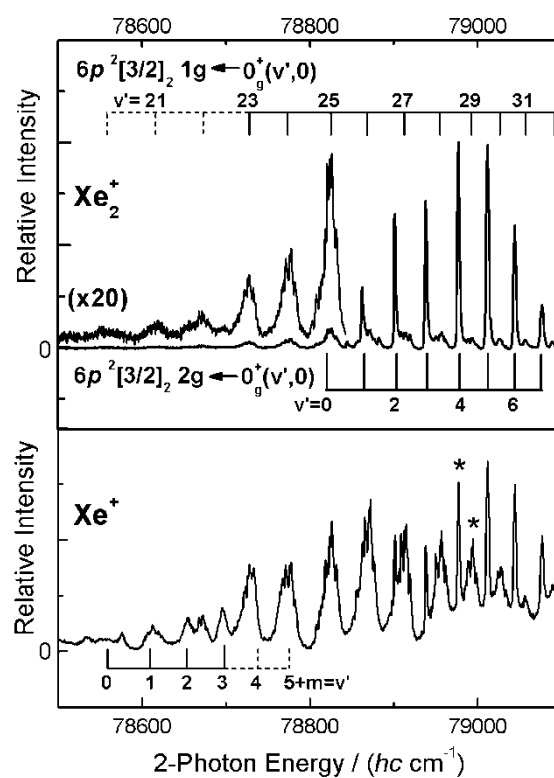


Figure 8

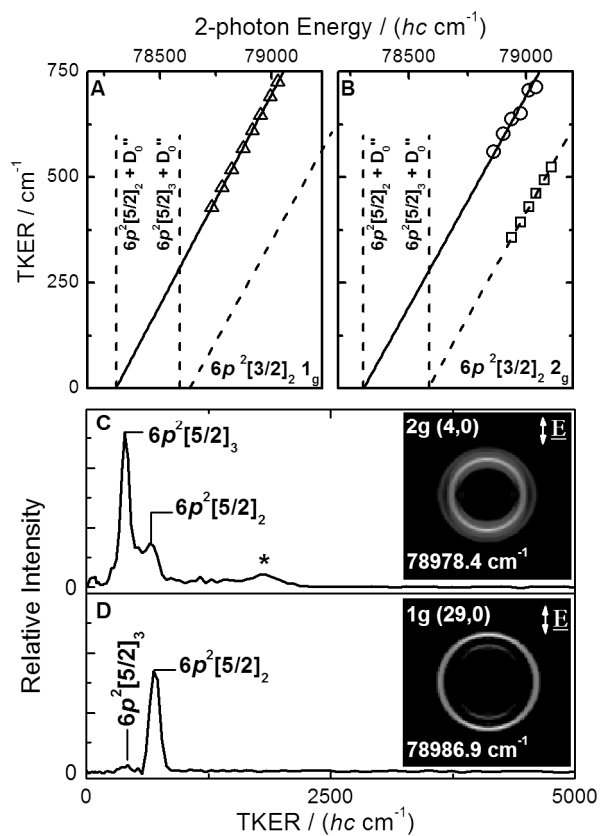


Figure 9

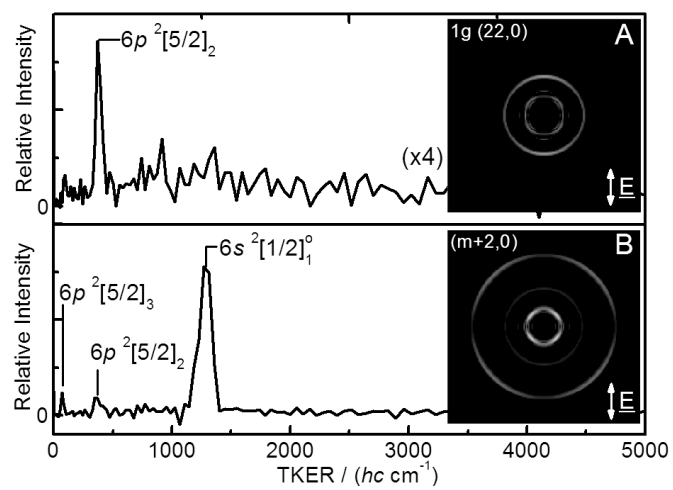


Figure 10

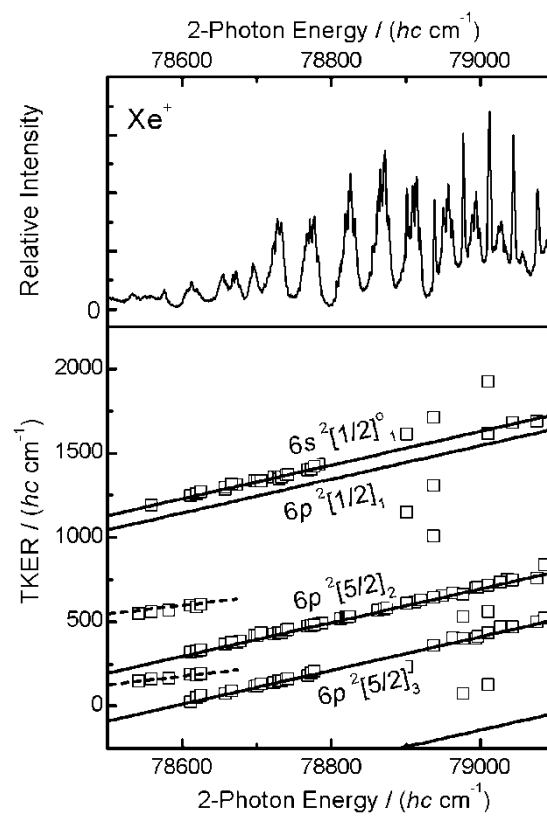


Figure 11

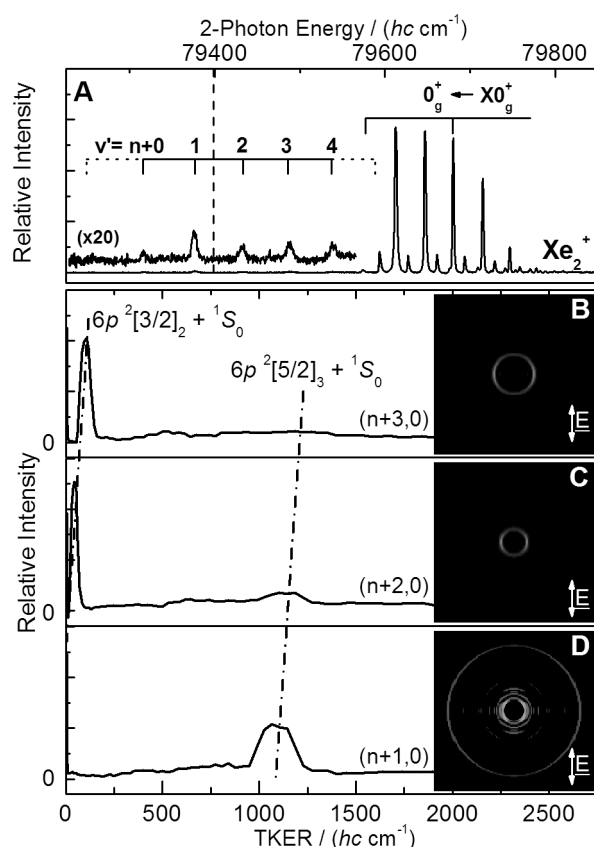


Figure 12

References

- ¹J.C. McLennan and R. Turnbull, Proc. Roy. Soc. Lon. 139, 683 (1933).
- ²J.C. McLennan and R. Turnbull, Proc. Roy. Soc. Lon. 129, 266 (1930).
- ³P.M. Dehmer, S.T. Pratt, and J.L. Dehmer, J. Chem. Phys. 85, 13 (1986).
- ⁴R.H. Lipson, A.R. Hoy, and E. Chan, J. Chem. Phys. 90, 4664 (1989).
- ⁵S.S. Dimov, J.Y. Cai, and R.H. Lipson, J. Chem. Phys. 101, 10313 (1994).
- ⁶S.S. Dimov, X.K. Hu, D.M. Mao, and R.H. Lipson, Chem. Phys. Lett. 239, 332 (1995).
- ⁷X.K. Hu, D.M. Mao, S.S. Dimov, and R.H. Lipson, Phys. Rev. A 54, 2814 (1996).
- ⁸V.A. Shubert, M. Rednic, and S.T. Pratt, J. Chem. Phys. 132, 124108 (2010).
- ⁹W. Gornik, S. Kindt, E. Matthias, and D. Schmidt, J. Chem. Phys. 75, 68 (1981).
- ¹⁰P.M. Dehmer, S.T. Pratt, and J.L. Dehmer, J. Phys. Chem. 91, 2593 (1987).
- ¹¹M.C. Castex, J. Chem. Phys. 74, 759 (1981).
- ¹²D.E. Freeman, K. Yoshino, and Y. Tanaka, J. Chem. Phys. 61, 4880 (1974).
- ¹³J.W. Keto, H. Cai, M. Kykta, C. Lei, T. Moller, and G. Zimmerer, J. Chem. Phys. 107, 6080 (1997).
- ¹⁴X.K. Hu, D.M. Mao, S.S. Dimov, and R.H. Lipson, J. Chem. Phys. 106, 9411 (1997).
- ¹⁵X.K. Hu, D.M. Mao, S.S. Dimov, and R.H. Lipson, J. Chem. Phys. 106, 9419 (1997).
- ¹⁶D.M. Mao, X.K. Hu, Y.J. Shi, and R.H. Lipson, Chem. Phys. 257, 253 (2000).
- ¹⁷R.H. Lipson, P.E. Larocque, and B.P. Stoicheff, J. Chem. Phys. 82, 4470 (1985).
- ¹⁸D.M. Mao, X.K. Hu, S.S. Dimov, and R.H. Lipson, J. Mol. Spectrosc. 181, 435 (1997).
- ¹⁹X.K. Hu, D.M. Mao, S.S. Dimov, and R.H. Lipson, Chem. Phys. 201, 557 (1995).
- ²⁰D.S. Green and S.C. Wallace, J. Chem. Phys. 100, 6129 (1994).
- ²¹W. Gornik, E. Matthias, and D. Schmidt, J. Phys. B-At. Mol. Opt. Phys. 15, 3413 (1982).
- ²²P. Slavicek, R. Kalus, P. Paska, I. Odvarkova, P. Hobza, and A. Malihevsky, J. Chem. Phys. 119, 2102 (2003).
- ²³C. Jonin, P. Laporte, and F. Spiegelmann, J. Chem. Phys. 117, 3049 (2002).
- ²⁴C. Jonin and F. Spiegelmann, J. Chem. Phys. 117, 3059 (2002).
- ²⁵O. Vallee, N. Tranminh, and J. Chapelle, J. Chem. Phys. 73, 2784 (1980).
- ²⁶W.C. Ermler, Y.S. Lee, K.S. Pitzer, and N.W. Winter, J. Chem. Phys. 69, 976 (1978).
- ²⁷W.R. Wadt, P.J. Hay, and L.R. Kahn, J. Chem. Phys. 68, 1752 (1978).
- ²⁸W.R. Wadt, J. Chem. Phys. 68, 402 (1978).
- ²⁹R.S. Mulliken, J. Chem. Phys. 52, 5170 (1970).

- ³⁰J.F. Castillo and K.L. Reid, *Laser Chem.* 19, 57 (1999).
- ³¹R.A. Aziz and M.J. Slaman, *Mol. Phys.* 57, 825 (1986).
- ³²H.A. Koehler, D.L. Redhead, Ferderbe.Lj, and P.J. Ebert, *Appl. Phys. Lett.* 21, 198 (1972).
- ³³A.W. Johnson and J.B. Gerardo, *J. Appl. Phys.* 45, 867 (1974).
- ³⁴J.K. Rice and A.W. Johnson, *J. Chem. Phys.* 63, 5235 (1975).
- ³⁵D.E. Freeman, K. Yoshino, and Y. Tanaka, *J. Chem. Phys.* 67, 3462 (1977).
- ³⁶W.S. Hopkins and S.R. Mackenzie, *J. Chem. Phys.* 134 (2011).
- ³⁷V.A. Shubert and S.T. Pratt, *J. Chem. Phys.* 134, 044315 (2011).
- ³⁸Y. Lu, Y. Morioka, T. Matsui, T. Tanaka, H. Yoshii, R.I. Hall, T. Hayaishi, and K. Ito, *J. Chem. Phys.* 102, 1553 (1995).
- ³⁹K. Vasilatou, U. Hollenstein, and F. Merkt, *Mol. Phys.* (2010).
- ⁴⁰W.S. Hopkins, S.M. Hamilton, P.D. McNaughter, and S.R. Mackenzie, *Chem. Phys. Lett.* 483, 10 (2009).
- ⁴¹W.S. Hopkins, A.P. Woodham, R.J. Plowright, T.G. Wright, and S.R. Mackenzie, *J. Chem. Phys.* 132, 9 (2010).
- ⁴²A. Eppink and D.H. Parker, *Re. Sci. Instrum.* 68, 3477 (1997).
- ⁴³G.M. Roberts, J.L. Nixon, J. Lecointre, E. Wrede, and J.R.R. Verlet, *Re. Sci. Instrum.* 80, 053104 (2009).
- ⁴⁴R.N. Dixon, *J. Chem. Phys.* 122, 13 (2005).
- ⁴⁵o.p.c.a.a.p.F.i.o.S.M. See Supplementary Material Document No._____ for Xe_2 photodissociation wavenumbers, see <http://www.aip.org/pubservs/epaps.html>.